PHYSICAL REVIEW C **83**, 021303(R) (2011)

Bent three-α linear-chain structure of ^{13}C

N. Furutachi
Meme Media Laboratory, Hokkaido University 060-8628 Sapporo, Japan

M. Kimura
Creative Research Initiative (CRIS), Hokkaido University, Sapporo 001-0021, Japan

(Received 9 October 2010; published 11 February 2011)

The stability of the three-α linear-chain structure of ^{13}C has been investigated with a microscopic $3\alpha + n$ model. We have found two excited rotational bands that have developed a three-α cluster structure in ^{13}C. The lower band built on $3/2^-_2$ state at 11.4 MeV has the bent three-α linear-chain structure, and this structure is stable against the bending motion of three-α clusters.

DOI: 10.1103/PhysRevC.83.021303 PACS number(s): 21.10.Re, 21.60.Gx, 27.20.+n

The linear-chain structure of α clusters has been discussed for a long time. In the past, the linear-chain configuration of three-α (3α) clusters was suggested in ^{12}C, and 0^+_2 state at $E_x = 7.65$ MeV was a candidate of this structure. Now, this state is known to have the dilute gas-like 3α structure that is interpreted as an α-condensed state [1,2]. Theoretically, another 0^+ state that has a large spectroscopic factor in the ^{8}Be$(2^+) + \alpha$ channel has been proposed around $E_x \sim 11$ MeV [3–6]. The studies with antisymmetrized molecular dynamics (AMD) [4,6] showed that this state has the bent linear-chain structure.

Search for a 3α linear-chain structure has been extended to C isotopes. The candidates have been suggested in ^{13}C based on the analysis of transfer reactions, inelastic excitations, and other experiments [7]. Theoretically, Itagaki *et al.* [8] discussed the stability of the linear-chain configuration in C isotopes based on a molecular-orbital model. They found that the linear-chain configuration is stable in ^{16}C with the assistance of the valence neutrons in the σ molecular orbital. They also investigated the linear-chain configuration in ^{13}C by using a $3\alpha + n$ model [9], and found the candidates of the observed band [7], which may have a linear-chain configuration.

Although Itagaki *et al.* [9] suggested the linear-chain state of ^{13}C, its structure and stability are still unclear. Therefore, in this Rapid Communication, we investigate the 3α cluster structure in excited states of ^{13}C by using a microscopic $3\alpha + n$ cluster model. We will show that there are two excited rotational bands with developed 3α cluster structure, one of them, built on the $3/2^-_2$ state, has the bent 3α linear-chain structure. The stability of this structure is investigated by the analysis of the energy surfaces as functions of the bending angle and the α-α distance. In this band, the valence neutron makes the intercluster distance between α clusters smaller, and the orthogonality to the ground band hinders the bending motion of the 3α clusters. The stability of the linear-chain configuration is achieved by these effects.

In this study, a microscopic $3\alpha + n$ cluster model was used. This model is based on the generator coordinate method (GCM) with the generator coordinate of 3α configuration. The valence neutron wave function is described by a sum of Gaussian wave packets with different widths.

The Hamiltonian is given as $\hat{H} = \hat{T} + \hat{V}_n + \hat{V}_c - \hat{T}_g$, where $\hat{T}$ is the total kinetic energy and $\hat{T}_g$ is the energy of the center-of-mass motion. We used Volkov No. 2 force [10] for the central part and G3RS force [11] for the spin-orbit part of the effective nuclear force $\hat{V}_n$. The Majorana parameter of Volkov No. 2 force and the strength of G3RS force are, respectively, $m = 0.6$ and $u_{ls} = 2000$ MeV, which reproduce the scattering phase shifts of $\alpha + n$ and $\alpha + \alpha$ systems [12].

We employ the parity projected $3\alpha + n$ wave function $\Phi^\pi = \hat{P}^\pi \Phi_{\rm int}$ as a variational function. In this study, we investigate only negative-parity states, $\pi = -$. The intrinsic wave function $\Phi_{\rm int}$ is given as

$$\Phi_{\rm int}(S) = \mathcal{A}[\varphi_\alpha(\boldsymbol{S}_1)\,\varphi_\alpha(\boldsymbol{S}_2)\,\varphi_\alpha(\boldsymbol{S}_3)\,\varphi_n], \tag{1}$$

where 3α clusters are located at the positions $\boldsymbol{S}_1$, $\boldsymbol{S}_2$, and $\boldsymbol{S}_3$. The α clusters have $(0s)^4$ configuration oriented at the position $\boldsymbol{S}$ and the valence neutron wave function is described by a sum of Gaussians with different widths,

$$\varphi_\alpha(\boldsymbol{S}) = \psi^4_\alpha(\boldsymbol{S}) \prod_{i=1}^{4} \eta_i, \tag{2}$$

$$\psi_\alpha(\boldsymbol{S}) = \exp\left\{-\frac{(\boldsymbol{r} - \boldsymbol{S})^2}{2b^2}\right\}, \tag{3}$$

$$\eta_i = \{p\uparrow, p\downarrow, n\uparrow, n\downarrow\}, \tag{4}$$

$$\varphi_n = \sum_{m=1}^{M} C_m \phi_m(\boldsymbol{Z}_m)\chi_m\tau_n, \tag{5}$$

$$\phi_m(\boldsymbol{Z}_m) = \exp\left[-\frac{(\boldsymbol{r} - \boldsymbol{Z}_m)^2}{2\nu_m^2}\right], \tag{6}$$

$$\chi_m = \left(\frac{1}{2} + \xi_m\right)\chi_\uparrow + \left(\frac{1}{2} - \xi_m\right)\chi_\downarrow, \tag{7}$$

$$\tau_n = \text{neutron}. \tag{8}$$

The width parameter b of the α-cluster wave function is fixed to 1.46 fm, and the number of superposed Gaussian wave packets of the valence neutron wave function is $M = 6$, which is enough to achieve the energy convergence. The variational parameters C_m, ν_m, $\boldsymbol{Z}_m$, and ξ_m of the valence neutron wave function φ_n are optimized by the energy variation for each 3α

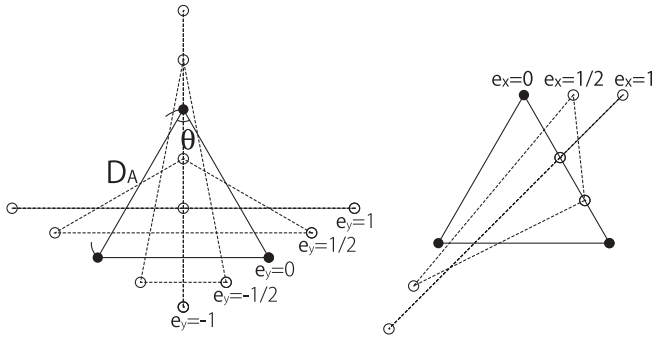

FIG. 1. 3α configurations for GCM bases and the definitions of D_A and θ. Details of 3α configurations are given in Ref. [3].

configuration $S = \{\boldsymbol{S}_1, \boldsymbol{S}_2, \boldsymbol{S}_3\}$. Here the configurations of 3α clusters S are the same as those used in the 3α GCM study for ^{12}C [3]. 3α configurations are represented by the inter-α distance parameter D_A and the coordinates e_x and e_y. Definitions of D_A, e_x, and e_y are given in Fig. 1. D_A ranges from 1 fm to 6 fm, and the adequate e_x and e_y are chosen for each D_A: $[D_A = 1$ fm, $(e_y = e_x = 0)]$, $[D_A = 2,\ (e_y = 0, \pm 1/2)]$, $[D_A = 3,\ (e_y = 0, \pm 1/2, 1)]$, $[D_A = 4,\ (e_y = 0, \pm 1/3, \pm 2/3, 1)$, $(e_x = 1/2)]$, $[D_A = 5,\ (e_y = 0, \pm 1/3,\ 1/2,\ \pm 2/3)$, $(e_x = 1/3,\ 2/3)]$, $[D_A = 6, (e_y = 0, \pm 1/3,\ 1/2,\ \pm 2/3)$, $(e_x = 1/3,\ 2/3)]$.

After the energy variation, we perform the angular momentum projection,

$$\Phi^{J-}_{MK}(S) = \hat{P}^J_{MK}\Phi^-(S). \tag{9}$$

Then they are superposed using 3α configuration S as the generator coordinate. The GCM wave function Ψ^{J-}_α is given as

$$\Psi^{J-}_\alpha = \sum_{SK} f_{SK\alpha}\Phi^{J-}_{MK}(S), \tag{10}$$

where the energy eigenvalue and coefficient $f_{SK\alpha}$ are determined by solving Hill-Wheeler equation [13]. The excitation energies, band structures, and other physical quantities discussed below are those obtained by this GCM calculation.

To discuss the stability of the 3α linear-chain structure, we investigate the energy surface that is orthogonal to the yrast state. First, we construct the wave function $\widetilde{\Phi}^{J-}_M(S)$ that has the 3α configuration S and is orthogonal to the yrast state. Denoting the wave function of the yrast state obtained by the GCM calculation as Ψ^{J-}_0, $\widetilde{\Phi}^{J-}_M(S)$ is given as

$$\widetilde{\Phi}^{J-}_M(S) = \bar{\Phi}^{J-}_M(S) - \langle\Psi^{J-}_0|\bar{\Phi}^{J-}_M(S)\rangle\Psi^{J-}_0, \tag{11}$$

$$\bar{\Phi}^{J-}_M(S) = \sum_K g_K\Phi^{J-}_{MK}(S), \tag{12}$$

where g_K is determined by diagonalizing the Hamiltonian. Since we perform this procedure for isosceles triangular configurations, we denote this wave function as $\widetilde{\Phi}^{J-}_M(D_A, \theta)$. An energy surface that is orthogonal to the yrast state is defined as the energy of $\widetilde{\Phi}^{J-}_M(D_A, \theta)$ as function of D_A and θ,

$$\widetilde{E}^{J-}(D_A, \theta) = \frac{\langle\widetilde{\Phi}^{J-}_M|\hat{H}|\widetilde{\Phi}^{J-}_M\rangle}{\langle\widetilde{\Phi}^{J-}_M|\widetilde{\Phi}^{J-}_M\rangle}. \tag{13}$$

We also compare $\widetilde{E}^{J-}(D_A, \theta)$ with that obtained without the orthogonality condition,

$$E^{J-}(D_A, \theta) = \frac{\langle\bar{\Phi}^{J-}_M|\hat{H}|\bar{\Phi}^{J-}_M\rangle}{\langle\bar{\Phi}^{J-}_M|\bar{\Phi}^{J-}_M\rangle}. \tag{14}$$

The overlap between the GCM wave function of the nonyrast state Ψ^{J-}_α and $\bar{\Phi}^{J-}_M(D_A, \theta)$ is also used in the discussion,

$$O^{J-}_\alpha(D_A, \theta) = \left|\langle\Psi^{J-}_\alpha|\bar{\Phi}^{J-}_M(D_A, \theta)\rangle\right|^2. \tag{15}$$

It is noted that this procedure is performed only for the analysis of the nonyrast GCM wave function Ψ^{J-}_α.

In the present calculation, we have obtained three rotational bands including the ground band. Among them, two excited rotational bands have pronounced a 3α cluster structure, and one of them has the 3α linear-chain structure with a small bending angle.

In Fig. 2, the negative-parity rotational bands obtained by the present calculation are compared with the observed ground band and $K^\pi = 3/2^-$ band proposed by Milin *et al.* [7]. The energies are measured from $3\alpha + n$ threshold energy. The experimental and calculated $3\alpha + n$ threshold energies are, respectively, -84.9 and -82.7 MeV. While the ground-state energy is well reproduced, $5/2^-_1$ and $7/2^-_1$ states disagree with the observation. This result is considered to be due to the limitation of the present model space (assumption of 3α clusters). Two excited rotational bands are built on $3/2^-_2$ (-0.3 MeV) and $3/2^-_3$ (2.8 MeV) states that are around the threshold energy. We shall call them $K^\pi = 3/2^-_2$ and $3/2^-_3$ bands. Both bands have quite a large moment of inertia and pronounced 3α cluster structure as will be shown later. Therefore, they are candidates of the observed $K^\pi = 3/2^-$ band [7]. We have found a $1/2^-_2$ state around the $3\alpha + n$ threshold. Since this state has a different structure from those of $K^\pi = 3/2^-_2$ and $3/2^-_3$ band, we have not classified this state as a band.

Milin *et al.* [7] also has proposed a positive-parity band that has the α clustering, and they interpreted the positive- and

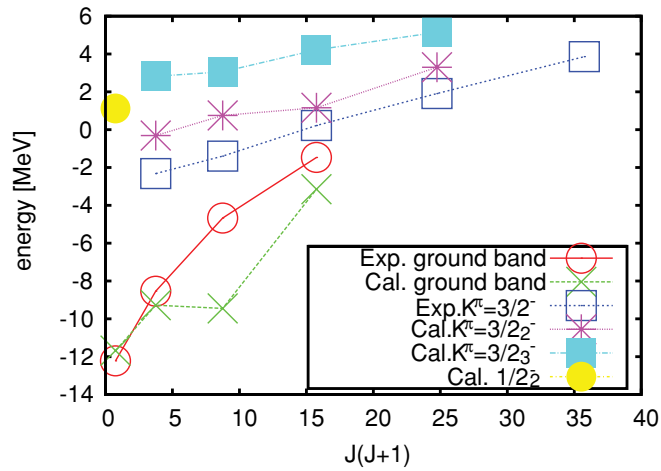

FIG. 2. (Color online) Calculated bands of ^{13}C. The energies are measured from $3\alpha + n$ threshold energy. $K^\pi = 3/2^-$ band proposed by Milin *et al.* [7] is also shown.

TABLE I. Energy, radius, and principal quantum number of the proton wave function for the ground state and two rotational bands of ^{13}C. The 0^+ states of ^{12}C are also shown for a comparison.

Band	J^π	E [MeV]	$\sqrt{\langle r_m^2\rangle}$ [fm]	N_p
g.s.	$1/2_1^-$	−11.7	2.41	4.7
$K^\pi = 3/2_2^-$	$3/2_2^-$	−0.3	3.24	10.7
	$5/2_2^-$	0.7	3.29	11.2
	$7/2_2^-$	1.2	3.20	10.3
	$9/2_1^-$	3.3	3.27	11.0
$K^\pi = 3/2_3^-$	$3/2_3^-$	2.8	3.20	10.4
	$5/2_3^-$	3.1	3.05	9.0
	$7/2_3^-$	4.2	3.19	10.3
	$9/2_2^-$	5.1	3.22	10.6
^{12}C	0_1^+	−5.2	2.53	5.4
	0_2^+	1.8	3.53	13.2
	0_3^+	5.6	3.61	14.1

negative-parity bands as a parity doublet band of ^{9}Be(g.s) + α cluster structure. A detailed theoretical investigation of positive-parity states is necessary, and will be a future work.

Table I shows the energy, radius, and principal quantum number of the proton wave function for each state. The principal quantum number N_p is evaluated from the expectation value of the harmonic oscillator Hamiltonian. The member states of $K^\pi = 3/2_2^-$ and $3/2_3^-$ bands have much larger matter radii and N_p than those of the ground state that originate in the pronounced 3α cluster structure of them. However, they are smaller than those of the 0_2^+ state of ^{12}C. As discussed below, the $3\alpha + n$ cluster structure of ^{13}C is not so dilute as the 0_2^+ state of ^{12}C.

To discuss the structure of the excited rotational bands, we have investigated the $3/2^-$ state energy surface that is orthogonal to the yrast state and the overlap between the GCM wave function and the wave functions on the energy surface. From these analyses, we have found that $3/2_2^-$ state is not so dilute as the 0_2^+ state of ^{12}C, but more stable against the bending motions of 3α clusters.

Figure 3 shows the energy surfaces of the $3/2^-$ state of ^{13}C and the 0^+ state of ^{12}C that are orthogonal to each yrast state. ^{13}C has the energy minimum at $(D_A, \theta) = (3.5\text{ fm}, 142^\circ)$ and ^{12}C has it at (4.0 fm, 142°). These minima correspond to the 3α configuration slightly bended from the linear-chain. These energy minima appear due to the orthogonality to the yrast states, which is approximately located at $(D_A, \theta) \sim$ (2.5 fm, 60°) in ^{13}C and (3.0 fm, 60°) in ^{12}C. Figure 4 shows the sections of the energy surfaces as functions of θ and D_A, and they are compared with those without the orthogonality condition. While the orthogonality condition is not important in the energy surface as a function of D_A, the minima at $\theta = 142^\circ$ in ^{12,13}C emerge due to the orthogonality condition that results in the large peak at $\theta = 60^\circ$.

The stability of the 3α configurations found on these minima against the motions of α clusters can be discussed

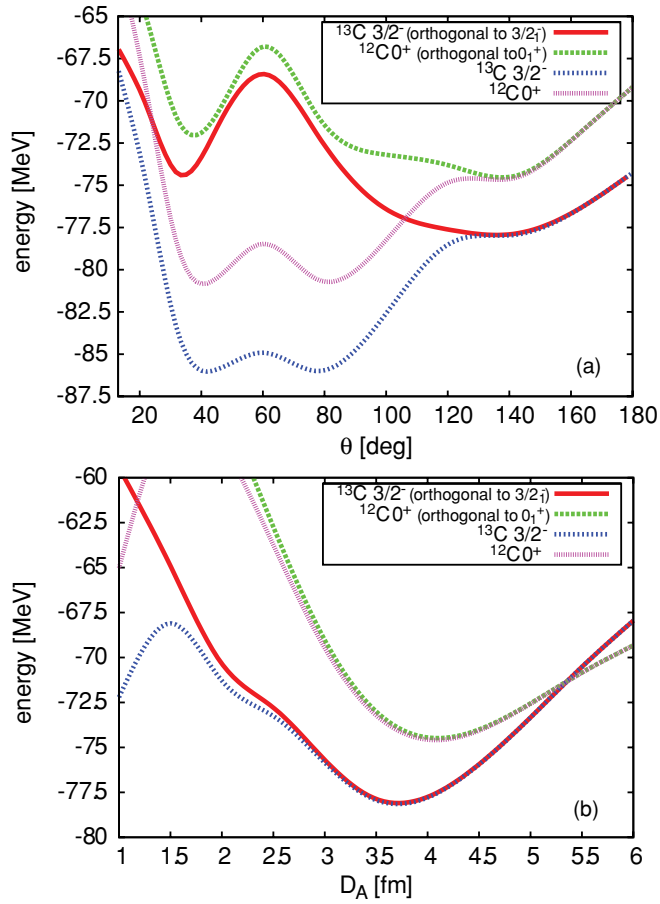

FIG. 4. (Color online) (a) Energy surfaces of ^{13}C and ^{12}C as function of θ. D_A is fixed to 3.5 fm for $3/2^-$ state of ^{13}C and 4.0 fm for 0^+ state of ^{12}C. (b) Energy surfaces as a function of D_A. θ is fixed to 142° for both ^{12}C and ^{13}C.

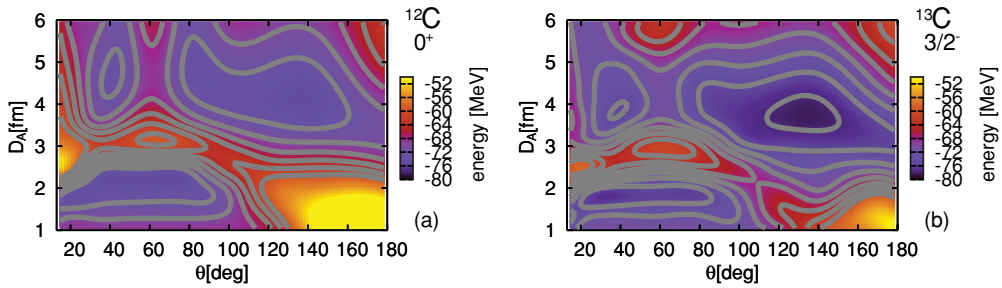

FIG. 3. (Color online) Energy surfaces of (a) $3/2^-$ state of ^{13}C and (b) 0^+ states of ^{12}C that are calculated using the wave functions orthogonal to $3/2_1^-$ and 0_1^+ states, respectively.

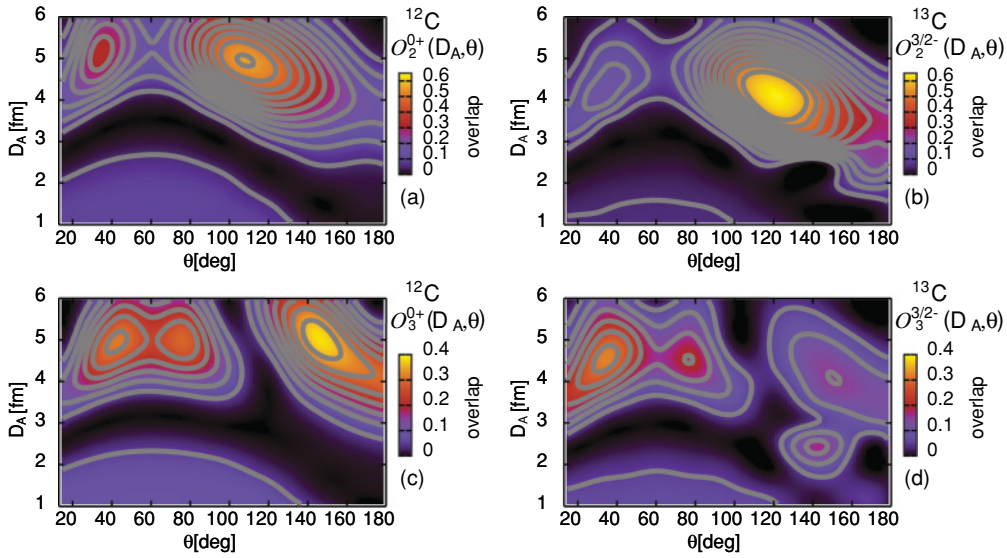

FIG. 5. (Color online) Overlaps between the GCM wave functions and the wave functions on the energy surface of (b) $3/2_2^-$ and (d) $3/2_3^-$ states. For a comparison, those for (a) 0_2^+ and (c) 0_3^+ states of ^{12}C are also shown.

by the behavior of the energy surfaces as functions of D_A and θ. Figures 4(a) and 4(b) shows the energy surfaces of ^{13}C that are orthogonal to the yrast state. They are steeper than those of ^{12}C in $60^\circ < \theta < 140^\circ$ and $D_A > 3.5$ fm regions, respectively. This behavior of the energy surface implies that the 3α cluster structure of the $3/2_2^-$ state of ^{13}C is a not so dilute gas-like one as the 0_2^+ state of ^{12}C, but stable against an increase of the α-α distance and a bending of α clusters. This result is a consequence of the attraction brought about by the valence neutron that gives deeper energy at a smaller D_A, where the larger peak appears around $\theta \sim 60^\circ$ due to the orthogonality to the yrast state.

The stability of the bent linear-chain configuration is confirmed by the analysis of the overlaps. Figure 5 shows the overlap between the GCM wave function and $\bar{\Phi}^{J-}_M(D_A, \theta)$, which is understood as the contributions of $\bar{\Phi}^{J-}_M(D_A, \theta)$ with various 3α configurations to each excited state. In the case of $3/2_2^-$ state, the overlap strongly peaked around $\theta = 120^\circ$. This result indicates the stability of the bent 3α linear-chain configuration. On the contrary, the overlap for 0_2^+ state of ^{12}C is not sharply peaked and widely spread in various 3α configurations. Thus, the overlaps clearly show the different nature between the $3/2_2^-$ state of ^{13}C and the 0_2^+ state of ^{12}C. The overlaps for the $3/2_3^-$ state spread in small and large θ regions, which indicate that different 3α configurations are mixed in this state.

We note that the insufficient description of the ground band mentioned above may affect the stability of the bent linear-chain configuration. A shell-like structure is considered to be needed for the reproduction of the ground band, and the inclusion of such structure will change the wave functions of the ground band. It leads to the change of the orthogonality condition that is important for the stability of the bent linear-chain structure.

We complete our study with the analysis of the valence neutron orbital. Figure 6(a) shows the valence neutron density of $\Phi_{\rm int}(D_A = 4$ fm, $\theta = 120^\circ)$ that has the maximum overlap with the $3/2_2^-$ state. This orbital can be interpreted with the molecular-orbital picture [14]. In Ref. [8], the orbital around the 3α clusters is classified into the π or σ orbital. The orbital shown in Fig. 6(a) corresponds to the π orbital that consists of three p-orbitals perpendicular to the vector that connects α clusters [Fig. 6(c)]. By adding the valence neutron in this orbital, the α-α distance shrinks and the binding energy of the system increases. As a consequence, the stability of the bent linear-chain configuration is achieved.

The valence neutron density of $\Phi_{\rm int}(D_A = 4.5$ fm, $\theta = 32^\circ)$ that has the maximum overlap with the $3/2_3^-$ state is shown in Fig. 6(b). The valence neutron orbital can be understood as a linear combination of the p-orbitals around α and ^{8}Be as

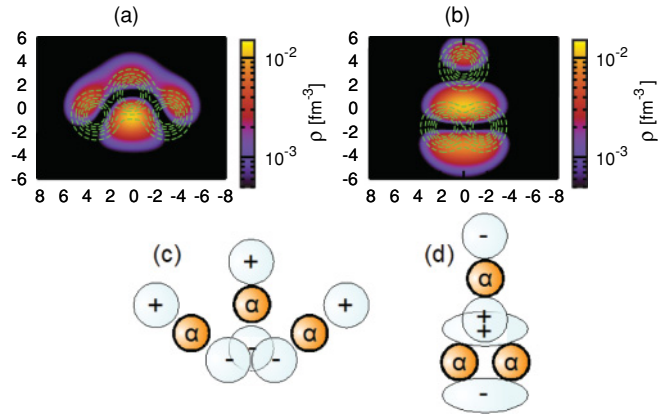

FIG. 6. (Color online) Density distributions and sketches of the molecular orbits. The wave functions of (a) and (b) have the maximum overlaps with the $3/2_2^-$ and $3/2_3^-$ states, respectively. Contour lines and color plots represent the density distributions of the most weakly bound one neutron and the remains. Units on boxes are fm. (c) and (d) sketches the molecular orbits of the wave functions of (a) and (b), respectively.

sketched in Fig. 6(d). However, since the overlap for the $3/2_3^-$ state indicates that different 3α configurations are mixed in this state, the interpretation of this state with the molecular-orbital picture may be insufficient.

In summary, we have investigated the 3α cluster structure of ^{13}C by using a $3\alpha + n$ cluster model to discuss the stability of the 3α linear-chain structure in this nucleus. We have obtained two excited rotational bands $K^\pi = 3/2_2^-$ and $3/2_3^-$ with pronounced α-cluster structures. They are built on $3/2_2^-$ and $3/2_3^-$ states around a $3\alpha + n$ threshold energy. Both bands have large moment of inertia and one of them may correspond to the observed band [7].

To understand the 3α cluster structure and its stability of these bands, the energy surface that is orthogonal to the yrast state was investigated. It was found that the orthogonality to the yrast state generates the energy minimum at large θ that corresponds to the bent 3α linear-chain configuration, and this configuration is more stable than that of the 0_2^+ state of ^{12}C. The stability of the bent linear-chain configuration is achieved by the attraction brought about by the valence neutron in the π orbital. The overlap with the GCM wave function has shown that the overlaps for the $3/2_2^-$ state are well localized around the energy minimum, while those of the 0_2^+ state of ^{12}C are widely spread in various 3α configurations. These results suggest the bent 3α linear-chain structure of $K^\pi = 3/2_2^-$ band of ^{13}C and the dilute gas nature of the 0_2^+ state of ^{12}C. The overlap with the $3/2_3^-$ state has shown that different 3α configurations are mixed in $K^\pi = 3/2_3^-$ band.

The numerical calculations were performed on the Altix3700 BX2 at YITP in Kyoto University.

[1] A. Tohsaki, H. Horiuchi, P. Schuck, and G. Röpke, Phys. Rev. Lett. **87**, 192501 (2001).
[2] P. Schuck, Y. Funaki, H. Horiuchi, G. Röpke, A. Tohsaki, and T. Yamada, Nucl. Phys. A **738**, 94 (2004).
[3] E. Uegaki, S. Okabe, Y. Abe, and H. Tanaka, Prog. Theor. Phys. **57**, 1262 (1977); **59**, 1031 (1978); **62**, 1621 (1979).
[4] Y. Kanada-En'yo, Prog. Theor. Phys. **117**, 655 (2007).
[5] M. Chernykh, H. Feldmeier, T. Neff, P. von Neumann-Cosel, and A. Richter, Phys. Rev. Lett. **98**, 032501 (2007).
[6] T. Suhara and Y. Kanada-En'yo, Prog. Theor. Phys. **123**, 303 (2010).
[7] M. Milin and W. von Oertzen, Eur. Phys. J. A **14**, 295 (2002).
[8] N. Itagaki, S. Okabe, K. Ikeda, and I. Tanihata, Phys. Rev. C **64**, 014301 (2001).
[9] N. Itagaki, W. von Oertzen, and S. Okabe, Phys. Rev. C **74**, 067304 (2006).
[10] A. B. Volkov, Nucl. Phys. **74**, 33 (1965).
[11] N. Yamaguchi, T. Kasahara, S. Nagata, and Y. Akaishi, Prog. Theor. Phys. **62**, 1018 (1979).
[12] S. Okabe and Y. Abe, Prog. Theor. Phys. **61**, 1049 (1979).
[13] D. L. Hill and J. A. Wheeler, Phys. Rev. **89**, 1102 (1953).
[14] Y. Abe, J. Hiura, and H. Tanaka, Prog. Theor. Phys. **49**, 800 (1973).